Contribution from the Departments of Chemistry, Tulane University, New Orleans, Louisiana 70118, University of Delaware, Newark, Delaware 19711, Louisiana State University, Baton Rouge, Louisiana 70803, Duquesne University, Pittsburgh, Pennsylvania 15282, and Washington State University, Pullman, Washington 99164

Crystal and Molecular Structures of Dihalotetrakis(pyrophosphito)diplatinum(III) Complexes. Integrative Use of Structural and Vibrational Data To Assess Intermetallic Bonding and the Trans Influence of the Pt(III)–Pt(III) Bond

KENNETH A. ALEXANDER,[1a] SAMUEL A. BRYAN,[1b] FRANK R. FRONCZEK,[1c] WILLIAM C. FULTZ,[1d] ARNOLD L. RHEINGOLD,[1d] D. MAX ROUNDHILL,*[1b] PAUL STEIN,[1e] and STEVEN F. WATKINS[1c]

Received November 9, 1984

The structures of $[N(C_4H_9)_4]_4[Pt_2(P_2O_5H_2)_4Br_2]$ (III), $K_4[Pt_2(P_2O_5H_2)_4I_2]$ (IV), and $K_2[N(C_4H_9)_4]_2[Pt_2(P_2O_5H_2)_4I_2]$ (V) show four P-bonded μ-pyrophosphito groups spanning axially halo-disubstituted diplatinum(III) centers. The Pt–Pt bond lengths vary as the halide (X) is $X^- = I^- > Br^- > Cl^-$, in accord with their σ-donating strength. In addition, the axial Pt–X bonds are long, reflecting a high trans influence for the Pt(III)–Pt(III) bond. Compound III is monoclinic, space group $P2_1/n$, with a = 16.047 (4) Å, b = 16.850 (3) Å, c = 16.331 (3) Å, β = 92.00 (2)°, V = 4413 (2) Å^3, and Z = 2; IV is tetragonal, space group $I4/m$, with a = 9.399 (1) Å, c = 15.777 (2) Å, V = 1393.7 (5) Å^3, and Z = 2; V is monoclinic, space group $P2_1/n$, with a = 9.749 (3) Å, b = 20.937 (8) Å, c = 15.242 (6) Å, β = 91.67 (3)°, V = 3110 (2) Å^3, and Z = 2. The trans influence for the Pt(III)–Pt(III) bond is estimated from vibrational spectroscopic data and found to be stronger than that for halides but weaker than that for methides, phenides, or hydrides.

Recently we have reported that the binuclear platinum(II) complex $K_4[Pt_2(P_2O_5H_2)_4]\cdot 2H_2O$ (I) will undergo oxidative addition of halogens X_2 (X = Cl, Br, I) to yield binuclear platinum(III) complexes $K_4[Pt_2(P_2O_5H_2)_4X_2]$.[2] These adducts have been characterized as dihalodiplatinum(III) complexes by elemental analysis, as well as by ^{31}P and ^{195}Pt NMR techniques, by UV–vis spectroscopy, and by Raman spectroscopy.[2] The complexes are diamagnetic. A single-crystal structure of the precursor platinum(II) complex $K_4[Pt_2(P_2O_5H_2)_4]\cdot 2H_2O$ shows a Pt–Pt separation of 2.925 (1) Å.[3-5] Although it was initially suggested that such an intermetallic spacing was indicative of a Pt–Pt bond,[4] a detailed vibrational analysis has concluded that any such bonding is very weak.[6] The simplified molecular orbital approach used by Gray considers the HOMO in these bimetallic d^8 complexes to be a la_{2u} ($d\sigma^*$) orbital. Complexes formed by oxidation reactions are therefore expected to have stronger homometallic bonds, since electrons are being removed from an antibonding orbital. In agreement with this premise, the axially substituted dichloro complex $K_4[Pt_2(P_2O_5H_2)_4Cl_2]$ (II) has a Pt(III)–Pt(III) intermetallic separation of 2.695 (1) Å,[3] which is significantly shorter than that found in $K_4[Pt_2(P_2O_5H_2)_4]\cdot 2H_2O$. No structural data have been reported for the bromo and iodo analogues $[Pt_2(P_2O_5H_2)_4X_2]^{4-}$ (X = Br, I). We now report the structures of these compounds and use observed distances in conjunction with vibrational data to evaluate the intermetallic bonding and to assess the trans influence of these Pt(III)–Pt(III) bonds.

The question of intermetallic bonding and its relation to the trans influence in these (pyrophosphito)diplatinum(III) complexes has been briefly discussed by us in the earlier vibrational spectroscopic study.[6] This earlier paper shows that, in addition to a shortening of the Pt–Pt separation on going from $K_4[Pt_2(P_2O_5H_2)_4]$ to $K_4[Pt_2(P_2O_5H_2)_4Cl_2]$, there is also an increase in the force constant (K(Pt–Pt)) of 0.9 mdyn/Å on going from $Pt_2(P_2O_5H_2)_4^{4-}$ to $Pt_2(P_2O_5H_2)_4X_2^{4-}$. Because of the lack of structural data on the bromo and iodo complexes at that time, if was necessary to carry out these force constant calculations on the two complexes $Pt_2(P_2O_5H_2)_4X_2^{4-}$ (X = Br, I) by making the inherent assumption that the stereochemistry of these bromo and iodo complexes was axial as found for the dichloro analogue. We had anticipated weak Pt–X bonds for these binuclear complexes in comparison with those of PtX_4^{2-} and PtX_6^{2-} complexes because of their low K(Pt–X) force constants.[6] These crystal structure determinations of $Pt_2(P_2O_5H_2)_4X_2^{4-}$ (X = Br, I) have confirmed our assumption of both axial stereochemistry and weak Pt–X bonds and have also shown that the Pt(III)–Pt(III) distances increase 0.059 (1) Å with Cl < Br < I. This article addresses similar questions to those considered by Lippard on structural comparisons in platinum(III) binuclear complexes of α-pyridone.[7] However, we extend the comparison of the trans influence of the Pt–Pt bond to include the very strong trans-directing hydride and methide ligands.

Experimental Section

Crystals of $[N(C_4H_9)_4]_4[Pt_2(P_2O_5H_2)_4Br_2]$ (III), $K_4[Pt_2(P_2O_5H_2)_4I_2]$ (IV), and $K_2[N(C_4H_9)_4]_2[Pt_2(P_2O_5H_2)_4I_2]$ (V), suitable for X-ray diffraction, were obtained by slow evaporation of aqueous solutions of $K_4[Pt_2(P_2O_5H_2)_4X_2]$ (X = Br, I)[2] either in the presence or absence of n-Bu_4NX (X = Br, I). The respective orange and red crystals were attached to a glass fiber with epoxy cement. Data for III and V were collected on a Nicolet R3 diffractometer using graphite-monochromated Mo Kα radiation. The reflections were collected by a $\omega/2\theta$ scan techniques over a range of 3.0–45.0° and 3.0–46.0° in 2θ. A summary of pertinent crystallographic parameters is presented in Table I.

The structures of III and V were solved and refined by using the Nicolet SHELXTL (Version 3.0) programs. A correction for Lp effects and an empirical absorption correction were applied to the data by using ψ-scan data from close to axial reflections (absorption coefficients 43.05 and 57.87 cm^{-1}, respectively). Data were corrected for absorption by refining a six-parameter defined pseudoellipsoid, which is then used to calculate the corrections (transmission coefficients, max/min = 0.049/0.031 and 0.100/0.046, respectively for III and V). A profile-fitting procedure was applied to the data to improve the precision of the measurement of weak reflections. No correction for decay was required.

The direct-methods technique (SOLV) yielded the heavy-atom positions of the Pt, P, and halogen atoms in each compound. All other non-hydrogen atoms were determined by difference Fourier techniques. All non-hydrogen atoms were refined anisotropically by using blocked-cascade, least-squares-refinement methods. The hydrogen atom positions were calculated in idealized positions on the basis of d(C–H) = 0.96 Å and thermal parameters equal to 1.2 times the isotropic equivalent value for the atom to which it was attached. The final discrepancy indices are $R(F)$ = 3.5% and $R_w(F)$ = 3.6% for both compounds. The final difference map for III showed a highest peak of 0.88 e Å^{-3} at a distance of 1.09 Å from the Pt atom, and the map for V showed a highest peak of 1.21 e Å^{-3} at a distance of 1.09 Å from the Pt atom.

For structure IV intensity data were collected on an Enraf-Nonius CAD4 diffractometer equipped with Mo Kα radiation and a graphite

(1) (a) Washington State University. (b) Tulane University. (c) Louisiana State University. (d) University of Delaware. (e) Duquesne University.
(2) Che, C. M.; Schaefer, W. P.; Gray, H. B.; Dickson, M. K.; Stein, P. B.; Roundhill, D. M. *J. Am. Chem. Soc.* **1982**, *104*, 4253–4255.
(3) Che, C. M.; Herbstein, F. H.; Schaefer, W. P.; Marsh, R. E.; Gray, H. B. *J. Am. Chem. Soc.* **1983**, *105*, 4604–4607.
(4) Filomena Dos Remedios Pinto, M. A.; Sadler, P. J.; Neidle, S.; Sanderson, M. R.; Subbiah, A.; Kuroda, R. *J. Chem. Soc., Chem. Commun.* **1980**, 13–15.
(5) Marsh, R. E.; Herbstein, F. H. *Acta Crystallogr., Sect. B: Struct. Sci.* **1983**, *B39*, 280–287.
(6) Stein, P.; Dickson, M. K.; Roundhill, D. M.; *J. Am. Chem. Soc.* **1983**, *105*, 3489–3493.
(7) Hollis, L. S.; Roberts, M. M.; Lippard, S. J. *Inorg. Chem.* **1983**, *22*, 3637–3644.

0020-1669/85/1324-2803$01.50/0

Table I. Crystal and Intensity Data Collection Summary

	III	IV	V
formula	$[N(C_4H_9)_4]_4[Pt_2(P_2O_5H_2)_4Br_2]$	$K_4[Pt_2(P_2O_5H_2)_4I_2]\cdot 2H_2O$	$K_2[N(C_4H_9)_4]_2[Pt_2(P_2O_5H_2)_4I_2]$
fw	1045.83	1412.3	1782.99
a, Å	16.047 (4)	9.399 (1)	9.749 (3)
b, Å	16.850 (3)		20.937 (8)
c, Å	16.331 (3)	15.777 (2)	15.242 (6)
β, deg	92.00 (2)		91.67 (3)
V, Å^3	4413 (2)	1893.7 (5)	3110 (2)
cryst syst	monoclinic	tetragonal	monoclinic
space group	$P2_1/n$	$I4/m$	$P2_1/n$
Z	2	2	2
ρ(calcd) g cm^{-3}	2.42	3.365	1.90
cryst dimens, mm	0.40 × 0.40 × 0.36	0.32 × 0.32 × 0.36	0.40 × 0.31 × 0.29
radiation[d]	Mo Kα	Mo Kα	
abs coeff (μ(Mo Kα)), cm^{-1}	43.05	134.6	57.87
temp, °C	25 ± 2	23	25 ± 2
scan speed, deg min^{-1}	4.0–2.0	0.48–5.0	3.0–12.0
scan type	$2\theta/\theta$		$2\theta/\theta$
scan range	$2.0 + \Delta(\alpha_1 - \alpha_2)$		$1.6 + \Delta(\alpha_1 - \alpha_2)$
stds monitored/reflcns	3/147		3/197
2θ limits, deg	3.0–45.0		3.0–46.0
reflcns collcd	$\pm h,k,l$		$\pm h,k,l$
no. of reflcns collcd	6443		4774
no. of unique reflcns	5343	1589	3974
no. of unique reflcns used with $F_o > 3\sigma$	4822; $n = 3$	1162	3571; $n = 3$
weighing factor, g[a]	0.000 33		0.000 32
$R(F)$[b]	0.035	0.028	0.035
$R_w(F)$[c]	0.036	0.039	0.036
GOF	1.488	1.537	
highest peak on final difference map, e Å^{-3}	0.88; 1.09 Å from Pt	1.24; 1.09 Å from Ppt	1.21; 1.09 Å from Pt

[a] $w = 1/[\sigma^2(F) + |g|(F^2)]$. [b] $R = \sum[|F_o| - |F_c|]/\sum|F_o|$. [c] $R_w = [\sum w^{1/2}(|F_o| - |F_c|)]/\sum w^{1/2}(F_o)$. [d] Graphite monochromated.

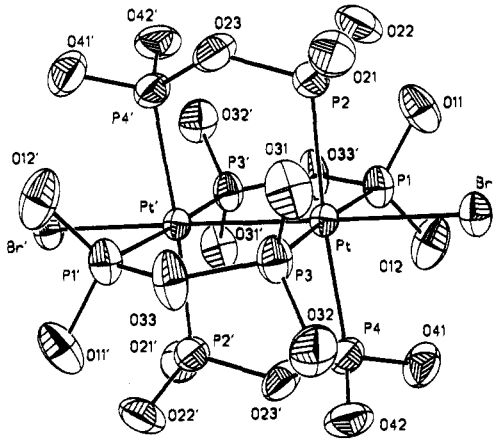

Figure 1. Thermal ellipsoid view of the $[Pt_2(P_2O_5H_2)_4Br_2]^{4-}$ (III) ion at 40% probability.

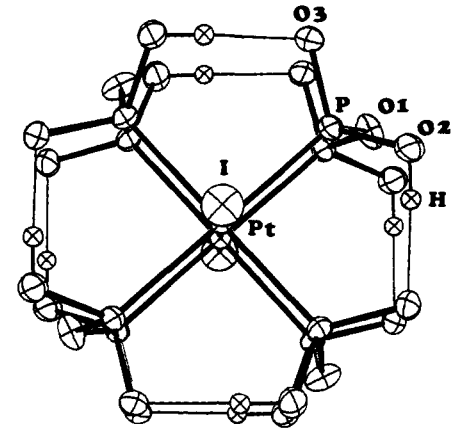

Figure 2. Thermal ellipsoid view of the $[Pt_2(P_2O_5H_2)_4I_2]^{4-}$ (IV) ion at 40% probability.

monochromator by $\omega/2\theta$ scans of variable rate designed to yield $\sigma(I) = 0.02I$ for all observable data. A maximum of 120 s was placed on the scan time for weak reflections. One octant of data was collected and corrected for Lp, background, and absorption effects. The absorption correction was based on ψ scans of reflections near $\chi = 90°$ with minimum relative transmission coefficient 71.6%. Data having $I > 3\sigma(I)$ were used in the refinement.

The data for IV are strongly pseudosymmetric to Laue group $4/mmm$, with $R = 0.10$ for averaging data across the diagonal mirror. The structure was initially solved by heavy-atom techniques in space group $I4/mmm$ and refined to $R = 0.13$, with the model exhibiting P atoms on the mirror at $y = 0$ and the bridging oxygen in POP, as well as one of the K atoms, disordered across that mirror. Degradation of the symmetry to $I4/m$ led to a completely ordered anion and location of its H atom. A substitutional disorder persists, in which a K^+ ion and water molecule share a site on the mirror plane at $z = 0$.

Refinement was by full-matrix least squares with weights $w = \sigma^{-2}(F_o)$, treating heavy atoms anisotropically and refining the H atom isotropically. A small secondary extinction coefficient (4.2 (3) × 10^{-7}) was necessary. Final residuals are given in Table I.

Results and Discussion

Structures of $(n\text{-}Bu_4N)_4[Pt_2(P_2O_5H_2)_4Br_2]$, $K_4[Pt_2(P_2O_5H_2)_4I_2]$, and $K_2(n\text{-}Bu_4N)_2[Pt_2(P_2O_5H_2)_4I_2]$. The single-crystal X-ray

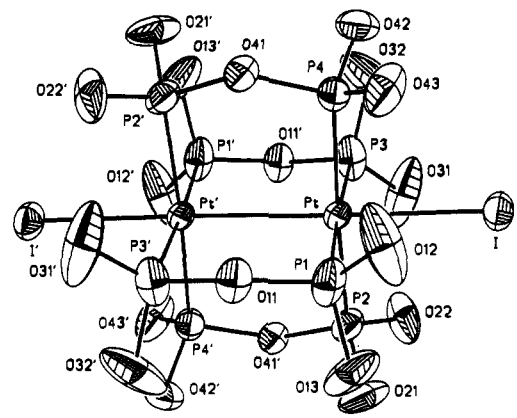

Figure 3. Thermal ellipsoid view of the $[Pt_2(P_2O_5H_2)_4I_2]^{4-}$ (V) ion at 40% probability.

structures of $(n\text{-}Bu_4N)_4[Pt_2(P_2O_5H_2)_4Br_2]$ (III), $K_4[Pt_2(P_2O_5H_2)_4I_2]$ (IV), and $K_2(n\text{-}Bu_4N)_2[Pt_2(P_2O_5H_2)_4I_2]$ (V) show the anions to have a stereochemistry analogous to that of $[Pt_2$-

Table II. Atomic Positional Coordinates (×10⁴) for the Anion $[Pt_2(P_2O_5H_5)_4Br_2]^{4-}$ (III)[a]

atom	x	y	z
Pt	9928 (1)	536 (1)	4381 (1)
Br	9794 (1)	1565 (1)	3220 (1)
P(1)	8590 (1)	71 (1)	3972 (1)
P(2)	9336 (1)	1488 (1)	5244 (1)
P(3)	11260 (1)	1082 (1)	4687 (1)
P(4)	10506 (1)	−353 (1)	3435 (1)
O(11)	7908 (3)	725 (3)	4039 (4)
O(12)	8512 (4)	−285 (4)	3128 (3)
O(21)	9807 (4)	2298 (3)	5228 (3)
O(22)	8416 (3)	1646 (3)	5111 (4)
O(23)	9490 (4)	1242 (3)	6198 (3)
O(31)	11261 (3)	1941 (3)	4946 (3)
O(32)	11864 (3)	984 (4)	3972 (3)
O(33)	11737 (3)	594 (3)	5408 (3)
O(41)	9945 (4)	−471 (3)	2649 (3)
O(42)	11377 (4)	−158 (3)	3184 (3)

[a] Estimated standard deviations in parentheses.

Table III. Atomic Potential Coordinates (×10⁴) for the Anion $[Pt_2(P_2O_5H_2)_4I_2]^{4-}$ (IV)[a]

atom	x	y	z
Pt	0	0	872.9 (2)
I	0	0	2613.3 (4)
P	2490 (1)	−173 (1)	918.9 (6)
O(1)	3112 (5)	−630 (6)	0
O(2)	3053 (4)	−1439 (4)	1468 (2)
O(3)	3292 (4)	1132 (4)	1196 (2)
H(O2)	2432 (70)	−2061 (70)	1401 (40)

[a] Estimated standard deviations in parentheses.

Table IV. Atomic Positional Coordinates (×10⁴) for the Anion $[Pt_2(P_2O_5H_2)_4I_2]^{4-}$ (V)[a]

atom	x	y	z
Pt	4955 (1)	311 (1)	9208 (1)
I	4838 (1)	912 (1)	7626 (1)
P(1)	4506 (3)	1283 (1)	9895 (2)
P(2)	7337 (2)	486 (1)	9273 (2)
P(3)	5419 (3)	−634 (1)	8453 (2)
P(4)	2572 (2)	164 (1)	9068 (2)
O(11)	4036 (6)	1187 (2)	10881 (4)
O(12)	3306 (10)	1659 (4)	9492 (4)
O(13)	5736 (9)	1739 (3)	9969 (5)
O(21)	7762 (6)	1167 (3)	9523 (5)
O(22)	8053 (6)	289 (4)	8429 (4)
O(31)	6585 (10)	−593 (3)	7807 (5)
O(32)	4157 (10)	−934 (3)	7979 (6)
O(41)	1943 (5)	−22 (2)	10007 (4)
O(42)	2114 (7)	−360 (4)	8438 (4)
O(43)	1796 (6)	779 (3)	8850 (5)

[a] Estimated standard deviations in parentheses.

$(P_2O_5H_2)_4Cl_2]^{4-}$ (II) with the halide ligands X-ray mutually axial. Each dianionic pyrophosphito ligand bridges equatorial coordination positions of the platinum(III) centers.

The labeling and molecular structures of the anions $[Pt_2(P_2O_5H_2)_4Br_2]^{4-}$ (III) and $[Pt_2(P_2O_5H_2)_4I_2]^{4-}$ (IV and V) are shown in Figures 1–3 respectively. Atomic coordinates are given in Tables II–IV. Selected bond distances and bond angles are presented in a comparative fashion in Table V. The bond distances and bond angles of the cations in III and V are consistent with those expected for tetra-*N*-butylammonium moieties.

Dimeric anions III and V are located about inversion centers such that half of each anion is found per asymmetric unit. Dimeric anion IV has crystallographic symmetry C_{4h}. Each Pt is pseudooctahedral with approximate square planes of P atoms in an eclipsed configuration. The other two positions of the octahedron are occupied by the halogen atom (III) Pt–Br = 2.572 (1) Å, (IV), Pt–I = 2.746 (1) Å, (V) Pt–I = 2.721 (1) Å) and the other Pt atom of the binuclear anion ((III) Pt–Pt = 2.716 (1) Å, (IV) Pt–Pt = 2.754 (1) Å, (V) Pt–Pt = 2.742 (1) Å).

The hydrogen atoms of the $(P_2O_5H_2)^{2-}$ ligands were not observed on the final difference maps for III. The terminal oxygen atoms of the ligand show a consistent short–long combination of P–O bond distances (P—O = 1.556 [4] (6) Å, P═O = 1.507[2](6) Å). For structure IV the hydrogen atom was observed on a difference map and refined. Again a short–long combination of P–O distances is found (P—O = 1.565 (3) Å, P═O = 1.504 (3) Å). The final difference map of V showed no peaks assignable to the hydrogen atoms of the ligand. Furthermore in V there is no clear distinction in the terminal P–O bond distances between the singly and doubly bonded entities (P–O distances = 1.535 [7] (9) and 1.525 [5] (9) Å). As with III, no attempt was made to include contributions from hydrogen atoms of the ligand in the structure of V. The crystal of V contains a 50:50 mixture of the potassium and tetra-*n*-butylammonium cations. The potassium ion is disordered within the cavity it occupies. This disorder was successfully modeled as a single potassium ion occupying two distinct locations. These positions refined independently to a separation distance (K(1)–K(2)) of 2.45 Å. Both potassium ions show similar oxygen contacts within the expected range (2.5–3.5 Å).

Before a detailed discussion of comparative distances in these pyrophosphito complexes can be made, the question of differences between the two structures of the anions $[Pt_2(P_2O_5H_2)_4I_2]^{4-}$ must be addressed. The structure of $K_4[Pt_2(P_2O_5H_2)_4I_2]\cdot 2H_2O$ (IV) is the "normal" one. This structure shows the alternating P—O and P═O distances found in I–III. The observed differences in these parameters are 6σ in I and II, 8σ in III, and 20σ in IV. The structure of V does not follow this pattern since the difference between the P—O and P═O distances is only 1σ and is therefore insignificant. Disorder may explain the lack of discrimination between the P═O and P—O bonds, but we cannot discount the possibility of intramolecular symmetric hydrogen bonds. The Pt–Pt–P angles in these complexes are all in the region of 92°, showing that the shortened Pt–Pt distance distorts the platinum atoms out of plane. For IV the tetragonal crystal symmetry requires all P–Pt–P angles between cis phosphorus atoms to be

Table V. Selected Bond Distances and Angles for $K_4[Pt_2(P_2O_5H_2)_4]\cdot 2H_2O$ (I), $K_4[Pt_2(P_2O_5H_2)_4Cl_2]$ (II), $(n\text{-}Bu_4N)_4[Pt_2(P_2O_5H_2)_4Br_2]$ (III), $K_4[Pt_2(P_2O_5H_2)_4I_2]$ (IV), and $K_2(n\text{-}Bu_4N)_2[Pt_2(P_2O_5H_2)_4I_2]$ (V)

	I "Pt_2"	II "Pt_2Cl_2"	III "Pt_2Br_2"	IV "Pt_2I_2"	V "Pt_2I_2"
Pt—Pt	2.925 (1)	2.695 (1)	2.716 (1)	2.754 (1)	2.742 (1)
Pt—P	2.320 (5)	2.350 [1] (2)	2.362 [3] (2)	2.348 (1)	2.343 [6] (2)
P—O(H)	1.579 (9)	1.557 [8] (7)	1.556 [4] (6)	1.565 (3)	1.535 [7] (9)
P═O	1.519 (9)	1.512 [7] (7)	1.507 [2] (6)	1.504 (3)	1.525 [5] (9)
P—O(bridging)	1.623 (6)	1.616 [8] (7)	1.613 [6] (5)	1.621 (2)	1.612 [10] (6)
Pt—X		2.407 (2)	2.572 (1)	2.746 (1)	2.721 (1)
Pt—Pt—P	90.67 (10)	92.17 [46] (5)	92.4 [4] (1)	91.77 (2)	91.6 [3] (1)
Pt—P—O(H)	114.0 (5)	113.9 [9] (3)	112.6 [3] (2)	114.02 (14)	113.9 [7] (3)
Pt—P═O	118.0 (5)	115.7 [10] (3)	115.7 [6] (2)	116.86 (14)	115.0 [3] (3)
Pt—P—O(bridge)	110.3 (4)	110.2 [10] (3)	110.8 [6] (2)	110.48 (16)	111.0 [8] (2)
P—O—P	133.3 (9)	125.5 [19] (4)	128.8 [24] (3)	126.87 (29)	125.5 [1] (4)
Pt—Pt—X		179.00	179.3	179.98 (8)	179.1

[a] Numbers in square brackets are root-mean-square derivations of the individual values (either 2 or 4 in number) from their mean.

Table VI. Comparative Pt–Pt and Pt–X (X = Cl, Br, I, NO_2) Distances in Pt(III)–Pt(III), Pt(IV), and Pt(II) Halo and Nitro Complexes

compd	Pt–X, Å	Pt–Pt, Å	ref
$K_4[Pt_2(P_2O_5H_2)_4Cl_2]$	2.407 (2)	2.695 (1)	3
$(n\text{-}Bu_4N)_4[Pt_2(P_2O_5H_2)_4Br_2]$	2.572 (1)	2.716 (1)	this work
$K_4[Pt_2(P_2O_5H_2)_4I_2]$	2.742 (1)	2.754 (1)	this work
$(Et_4N)_2[Pt_2(H_2PO_4)_2(HPO_4)_2Cl_2]\cdot H_2O$	2.448 (4)	2.529 (1)	9
$[Pt_2(NH_3)_4(C_5H_4NO)_2Cl_2](NO_3)_2$	2.444 (2), 2.429 (4)	2.568 (1)	7
$[Pt_2(NH_3)_4(C_5H_4NO)_2Br_2](NO_3)_2\cdot{}^1/_2H_2O$	2.573 (1), 2.562 (1)	2.582 (1)	7
K_2PtCl_6	2.323 (1)		14
$(Me_4N)_2[PtCl_6]$	2.293 (4)		15
K_2PtBr_6	2.464 (3)		16
Cs_2PtI_6	2.677 (1)		17
$(pyH)_2PtI_6$	2.661 (1)		18
K_2PtCl_4	2.316 (2)		19
Cs_2PtCl_4	2.294 (3), 2.304 (3)		20
Rb_2PtBr_4	2.435 (7)		21
K_2PtI_5 ($[PtI_4]^{2-}$)	2.650 (2), 2.654 (2)		22
cis-$[PtCl_2(PMe_3)_2]$	2.364 (8), 2.388 (9)		23
trans-$[PtHCl(PEtPh_2)_2]$	2.422 (9)		24

identical (89.95 (5)°). For III, and particularly for V, the *trans*-P–Pt–P axes are skewed to make the *cis*-P–Pt–P angles different. In V these angles are 92.6 [2] (1)° and 87.35 [25] (10)°. In structures I–IV, the anions have local or crystallographic 4-fold symmetry along the Pt–Pt axis, whereas in V the anion has only 2-fold symmetry with the bridging oxygens in the P–O–P group folding in alternating directions in the horizontal plane.

In the diplatinum(II) complex $K_4[Pt_2(P_2O_5H_2)_4]\cdot 2H_2O$ (I) the angles Pt–Pt–P are all close to a right angle (90.67 (10)°), whereas in the diplatinum(III) complexes II–V the shortened Pt–Pt distance causes the Pt–Pt–P angle to increase into the 91.5–92.5° range. The Pt–Pt distances in these diplatinum(III) complexes with the $(P_2O_5H_2)^{2-}$ ligand are all the range 2.69–2.76 Å. This distance is close to that found in metallic platinum (2.746 Å),[8] but it is considerably longer than the Pt(III)–Pt(III) distances found in bridging pyridonato (2.56 (2) Å),[7] phosphato and sulfato (2.48 (1) Å),[9] and trifluoroacetato (2.56 (1) Å)[10] complexes.

Significant differences are found in the Pt_2I_2 cores between structure IV and V. Comparison of the Pt–Pt distances ((IV) 2.754 (1) Å, (V) 2.742 (1) Å) and Pt–I ((IV) 2.746 (1) Å, (V) 2.721 (1) Å) distances between IV and V shows that the former differs by 12σ and the latter by 25σ between the two structures. Compared to that in IV, the Pt_2I_2 unit in V has contracted along the axial direction to give shorter distances for both Pt–Pt and Pt–I. In view of the similarities of alternating P–O distances of structure IV with those of I–III, the distances found for IV will be those used for comparative discussion rather than those found for the disordered anion V. We should note, however, that this decision is based entirely on this fact that compounds I–IVe have the same axial ligand symmetries. No inference should be made that the differences in Pt–Pt and Pt–I distances between compounds IV and V are caused by disorder, nor should it be construed that structure V is "wrong". We have no adequate explanation for the differences between IV and V other than they are different compounds because of changes in the cations and hence the crystals and their nonbonded interactions are not the same.

For the first time in these pyrophosphito complexes the hydrogen atom has been located on the difference maps of IV and refined. This atom forms a linear O···H–O hydrogen bond. The distance from the oxygen of P—O is 0.83 (6) Å, and that from the P=O is 1.71 (7) Å. The O–H–O angle is 176 (7)°. The cyclic pattern of hydrogen bonds between P—OH and P=O is shown in Figure 2.

Table VII. Comparative A_{1g} Raman Frequencies and Calculated Force Constants in Pt(III)–Pt(III), Pt(IV), and Pt(II) Halo Complexes

complex	$\nu_1(A_{1g})$, cm^{-1}	K(Pt–X), mdyn/Å	ref
$[Pt_2(P_2O_5H_2)_4Cl_2]^{4-}$	304	1.54	6
$[Pt_2(P_2O_5H_2)_4Br_2]^{4-}$	218	1.36	6
$[Pt_2(P_2O_5H_2)_4I_2]^{4-}$	194 (110)	1.03	6
$[PtCl_6]^{2-}$	344	2.25	22,23,24
$[PtBr_6]^{2-}$	207	1.8	22,23,24
$[PtI_6]^{2-}$	105.3	1.06	22,23
$[PtCl_4]^{2-}$	330	2.14	25
$[PtBr_4]^{2-}$	208	1.84	25
$[PtI_4]^{2-}$	155	1.35	25

For the series of complexes $[Pt_2(P_2O_5H_2)_4X_2]^{4-}$ (X = Cl, Br, I) the changes in Pt(III)–Pt(III) distance between pairs are 21σ and 38σ. The respective distances for X = Cl, Br, I are 2.695 (1), 2.716 (1), and 2.754 (1) Å. The corresponding distances for Pt–X in this sequence are 2.407 (2), 2.572 (1), and 2.746 (1) Å.[11]

Trans Influence Variations in the Pt(III)–Pt(III) Bond Lengths. The found Pt–Pt bond distances in these halodiplatinum(III) complexes show that changing the axial halogen substituent causes small but significant variations in the intermetallic separation. In Table VI we collected together the data for these (pyrophosphito)diplatinum(III) complexes, and for comparative purposes the data are listed along with literature data for (μ-pyridinato)diplatinum(III) complexes.[7] In conjunction with Lippard's comparison between μ-pyridinato and μ-sulfato complexes of diplatinum(III),[7] it is apparent that these μ-pyrophosphito complexes of diplatinum(III) have a long Pt–Pt separation. We agree with Lippard's conclusion that these groupings of Pt–Pt distances with different bridging ligands are primarily a reflection of the different ligand bite distances across a bridge and should not be taken as prima facie evidence for differences in metal–metal bond energy.

The trend in the Pt(III)–Pt(III) distances in $[Pt_2(P_2O_5H_2)_4X_2]^{4-}$ (X = Cl, Br, I) follows the sequence I > Br > Cl over the range 2.754 (1)–2.695 (1) Å. This order follows that which is expected if the halide ligands are placed in order of their trans influence[12] in mononuclear platinum complexes. The Pt(III)–Pt(III) dimers have a vacant σ^* (d_{z^2}) orbital. Increasing the ligand σ-donor strength, I > Br > Cl, could cause a weakening of the Pt–Pt bond via the σ^*-orbital participation. Furthermore, increased mixing of halide character according to I > Br > Cl in the $\sigma(d_{z^2})$Pt orbitals is evident from the trend of the UV ($d\sigma$–d^*) absorptions (I, 338 nm; Br, 305 nm; Cl, 282 nm).[2]

Axial Ligand Distances to Platinum. The platinum(III)–halogen distances in these binuclear complexes are very long when com-

(8) "Handbook of Chemistry and Physics", 48th ed., The Chemical Rubber Co.: Cleveland, OH, 1967–1968; p F146.

(9) Cotton, F. A.; Falvello, L. R.; Han, S. *Inorg. Chem.* **1982**, *21*, 1709–1710. Cotton, F. A.; Han, S.; Conder, H. L.; Walton, R. A. *Inorg. Chim. Acta.* **1983**, *72*, 191–193. Conder, H. L.; Cotton, F. A.; Falvello, L. R.; Han, S.; Walton, R. A. *Inorg. Chem.* **1983**, *22*, 1887–1891. Cotton, F. A.; Falvello, L. R.; Han, S. *Inorg. Chem.* **1982**, *21*, 2889–2891. Bancroft, D. P.; Cotton, F. A.; Falvello, L. R.; Han, S.; Schwotzer, W. *Inorg. Chim. Acta* **1984**, *87*, 147–153.

(10) Schagen, J. D.; Overbeek, A. R.; Schenk, H. *Inorg. Chem.* **1978**, *17*, 1938–1940.

(11) The crystal structure of $Na_8[Pt_2(P_2O_5H)_4(NO_2)_2]\cdot 18H_2O$ (Hedden, D.; Walkinshaw, M. D.; Roundhill, D. M. *Inorg. Chem.*, in press) has respective Pt–Pt and Pt–N distances of 2.7333 (3) and 2.153 (6) Å.

(12) Appleton, T. G.; Clark, H. C.; Manzer, L. E. *Coord. Chem. Rev.* **1973**, *10*, 335–422.

Table VIII. Comparison of ν_{Pt-CH_3} or ν_{Pt-Cl} (cm^{-1}) in Complexes with Trans Ligands Such As Cl, Br, I, P, As, Pt, CH_3, H, and Phenide (Ph)

compd	trans ligand (L)[a]	ν_{Pt-CH_3}	ν_{Pt-Cl}	ref
trans-$[PtCl(CH_3)L_2]$	Cl	557–559		31, 32
trans-$[PtBr(CH_3)L_2]$	Br	552		31, 32
trans-$[PtI(CH_3)L_2]$	I	546–551		31, 32
cis-$[PtCl(CH_3)L_2]$	P, As	523–535		31, 32
trans-$[Pt(CH_3)(ROCR')L_2]^+PF_6^-$	$-C(OR)R'$[b]	513–525 (R)		33
$[Pt_2(P_2O_5H_2)_4CH_3I]^{4-}$	Pt	489 (R)		6
$Pt(CH_3)_4L_2$	CH_3	470		31
$[PtCl_6]^{2-}$	Cl		345, 344 (R)	26
$[Pt(CN)_4Cl_2]^{2-}$	Cl		349, 330 (R)	34
$[PtCl_4]^{2-}$	Cl		325, 330 (R)	29
$PtCl_2(CH_3)_2L_2$	Cl		332	31
$[Pt_2(P_2O_5H_2)_4Cl_2]^{4-}$	Pt		295, 304 (R)	6
cis-$[PtCl(CH_3)L_2]$	P, As		284–294	31, 32
trans-$[PtCl(CH_3)L_2]$	CH_3		269–278	31, 32
trans-$[PtClX(PEt_3)_2]$	X = H, CH_3, Ph		269–274	35
$PtCl_2(CH_3)_2L_2$	CH_3		250–265	31, 32

[a] L = $P(CH_3)_2Ph$, $P(CH_3)Ph_2$;[31] $As(CH_3)_2Ph$;[32] $As(CH_3)_3$, $P(CH_3)_2Ph$.[33] [b] Alkoxycarbenes with R' = CH_3 or C_2H_5.

pared with other platinum–halogen distances. From the complexes collected in Table VI, including the μ-pyridonato complexes and homoleptic halide salts of Pt(II) and Pt(IV), the platinum (III)–halogen distances in these μ-pyrophosphito complexes are among the longest in the group. It is apparent for both the (μ-pyridonato)- and the (μ-pyrophosphito)diplatinum(III) complexes that the trans influence of the Pt(III)–Pt(III) bond is very high. In comparison, platinum hydride complexes, such as *trans*-$PtHCl(PEtPh_2)_2$, have a longer Pt–Cl distance. For these diaxially substituted halo complexes, the platinum orbitals (presumably $6p\sigma(z)$) involved in platinum(III)–halogen bonding can form bonding and antibonding combinations between the platinum atoms, thereby weakening the Pt–X bond. Hence the trans influence of a platinum(III)–platinum(III) bond may be synergistically related to donating strength of the axial ligands.

In Table VI are also collected literature values of Pt–X distances in both divalent platinum complexes $[PtX_4]^{2-}$ (X = Cl, Br, I) and tetravalent complexes $[PtX_6]^{2-}$ (X = Cl, Br, I). Inspection of these data show that the platinum–halogen distances are relatively consistent. Since we expect these distances to be sensitive to both the oxidation state and coordination number at platinum, it is possible that the effects cancel on increasing both the charge and coordination number on going from Pt(II) to Pt(IV). We must conclude therefore in the diplatinum(III) complexes that the long platinum(III)–halogen distances are a consequence of the intermetallic bond and not simply a reflection of charge or coordination geometry at platinum.

Force Constant and ν_{Pt-X} Probes to the Pt–Pt Bond Trans Influence. An alternative approach to comparing bond distances in assessing bond strengths is to compare vibrational frequencies or force constants. Raman and IR data for the complexes $[Pt_2(P_2O_5H_2)_4X_2]^{4-}$ (X = Cl, Br, I, CH_3I) have been reported as well as their Pt–X stretching force constants.[6] These data, as well as the literature values for the Raman and IR Pt–X stretching frequencies and force constants of $[PtX_6]^{2-}$ and $[PtX_4]^{2-}$ complexes, are collected in Table VII. Diagonal Pt–X stretching force constants were obtained from a general valence force field (GVFF) and determined from all the fundamental frequencies of these complexes. To the extent that force constants correlate with bond energies, it is apparent from the K(Pt–X) values that the Pt–X bonds in the complexes $[Pt_2(P_2O_5H_2)_4X_2]^{4-}$ are weak. As with Pt–X distances, the force constants do not differ appreciably between the respective monomeric anionic groups of divalent and tetravalent halo complexes, but the respective values of K(Pt–X) in $[Pt_2(P_2O_5H_2)_4X_2]^{4-}$ are lower by some 0.3–0.6 mdyn/Å. These lowerings of K(Pt–X) provide good additional support for claiming a high trans influence weakening of the Pt–X bonds in these binuclear platinum(III) complexes.

In an earlier paper[6] we showed that the Raman bands at 218 cm^{-1} in $[Pt_2(P_2O_5H_2)_4Br_2]^{4-}$ and at 194 cm^{-1} in $[Pt_2(P_2O_5H_2)_4I_2]^{4-}$ have considerable metal–metal stretching character, and hence these modes do not truly reflect a Pt–X vibration. Their high frequencies, which result from mixing with ν_{Pt-Pt} at about 150 cm^{-1}, do not provide a reliable comparison for Pt–Br or Pt–I bond energies. These results do not contradict our conclusions that the interplatinum(III) bond exerts a large trans influence weakening but reflect the danger of comparing frequencies rather than force constants. The IR-active Pt–X frequencies, which do not mix with ν_{Pt-Pt} in centrosymmetric binuclear complexes, are compared with the IR-active Pt–X stretching frequencies of $[PtX_6]^{2-}$ and $[PtX_4]^{2-}$ in Table VII and are found respectively, in the order $[PtX_6]^{2-} > [PtX_4]^{2-} > [Pt_2(P_2O_5H_2)_4X_2]^{4-}$, corresponding with the order of their diagonal force constants.

The trend in K(Pt–X) follows the sequence of Cl > Br > I in each of the three series of complexes. This trend can be interpreted as showing that the platinum–halogen bond strength decreases in the sequence Pt–Cl > Pt–Br > Pt–I. This sequence is the expected one if the results are compared with bond strength data for Pt–X derived from thermodynamic cycles,[13] although not the anticipated one of the "hard and soft" acid base theory for ligands being used without considering solvation effects.

The lack of force constant data prevents a comparison of the strength of the Pt–Pt bond trans influence with ligands other than halides. While ν_{Pt-Cl} in $[Pt_2(P_2O_5H_2)_4Cl_2]^{4-}$ is likely influenced

(13) Poe, A. J.; Vaidya, M. S. *J. Chem. Soc.* **1961**, 1023–1028.
(14) Williams, R. J.; Dillon, D. R.; Milligan, W. O. *Acta Crystallogr., Sect. B: Struct. Crystallogr. Cryst. Chem.* **1973**, *B29*, 1369–1372.
(15) Berg, R. W.; Sotofte, I. *Acta Chem. Scand.* **1978** *A32*, 241–244.
(16) Grundy, H. D.; Brown, I. D. *Can. J. Chem.* **1970**, *48*, 1151–1154.
(17) Thiele, G.; Mrozek, C.; Kammerer, D.; Wittman, K. *Z. Naturforsch., B: Anorg. Chem., Org. Chem.* **1983**, *38B*, 905–910.
(18) Thiele, G.; Wagner, D. *Z. Anorg. Allg. Chem.* **1978**, *446*, 126–130.
(19) Mais, R. H. B.; Owston, P. G.; Wood, A. M. *Acta Crystallogr., Sect B: Struct. Crystallogr. Cryst. Chem.* **1972**, *B28*, 393–399.
(20) Rodek, E.; Bartl, H.; Sterzel, W.; Platte, C. *Neutes Jahrb. Mineral., Monatsh.* **1979**, 81–85.
(21) Robek, E.; Sterzel, W.; Bartl, H.; Schuckmann, W. *Neues Jahrb. Mineral., Monatsh.* **1979**, 277–281.
(22) Thiele, G.; Mrozek, C.; Wittman, K.; Wirkner, H. *Naturwissenschaften* **1978**, *65*, 206–207.
(23) Messmer, G. C.; Amma, E. L.; Ibers, J. A. *Inorg. Chem.* **1967**, *6*, 725–730.
(24) Eisenberg, R.; Ibers, J. A. *Inorg. Chem.* **1965**, *4*, 773–778.
(25) Bosworth, Y. M.; Clark, R. J. H. *J. Chem. Soc., Dalton Trans.* **1974**, 1749–1761.
(26) Labonville, P.; Ferraro, J. R.; Wall, S. M. C.; Basile, L. J. *Coord. Chem. Rev.* **1972**, *7*, 257–287.
(27) Adams, D. M.; Gebbie, N. A. *Spectrochim. Acta* **1963**, *19*, 925–930.
(28) Verma, V. P.; Sharma, D. K.; Pandey, A. N. *Acta Cien. Indica* **1977**, *3*, 58–62.
(29) Goggin, P. L.; Mirk, J. *J. Chem. Soc., Dalton Trans.* **1974**, 1479–1483.
(30) Hendra, P. J. *J. Chem. Soc. A.* **1967**, 1298–1301.
(31) Ruddick, J. D.; Shaw, B. L. *J. Chem. Soc. A.* 1969, 2801–2808.
(32) Ruddick, J. D.; Shaw, B. L. *J. Chem. Soc. A.* 1969, 2964–2970.
(33) Chisholm, M. H.; Clark, H. C. *Inorg. Chem.* **1971**, *10*, 1711–1716.
(34) Jones, L. H.; Smith, J. M. *Inorg. Chem.* **1965**, *4*, 1677–1681.
(35) Adams, D. M.; Chatt, J.; Gerratt, J.; Westland, A. D. *J. Chem. Soc.* **1964**, 734–739.

by ν_{Pt-Pt}, the effect is apparently small. An even better ligand for probing the trans influence is a methyl group since ν_{Pt-CH} generally occurs between 500-560 cm^{-1}. Previously ν_{Pt-CH} has been reported for $[Pt_2(P_2O_5H_2)_4CH_3I]^{4-}$ at 489 cm^{-1}.[6] A 14-cm^{-1} shift of ν_{Pt-CH} with the $^{13}CH_3I$ isotope in $[Pt_2(P_2O_5H_2)_4{}^{13}CH_3I]^{4-}$ indicates a nearly pure methyl motion for this mode. In Table VIII we compare ν_{Pt-CH} and ν_{Pt-Cl} in a series of platinum complexes with ligands trans to CH_3 and Cl such as Cl, Br, I, P, As, ROCR', CH_3, H, and Ph. As previously, low ν_{Pt-CH} or ν_{Pt-Cl} implies a strong trans influence, while a high frequency implies a weak trans influence. As is seen, ν_{Pt-Cl} and ν_{Pt-CH} are observed at 349-250 and 559-470 cm^{-1}, respectively, indicating a large variation in frequency as a function of the trans ligand. High frequencies are observed when Cl, Br, or I are trans to the detector vibration, indicating a comparatively weak trans influence for these ligands, while low frequencies are observed when methide or hydride are trans ligands in accord with the accepted trans influence of these ligands. In comparison, the Pt-Pt bond in $[Pt_2(P_2O_5H_2)_4CH_3I]^{4-}$ and $[Pt_2(P_2O_5H_2)_4Cl_2]^{4-}$ shows a trans influence that is stronger than that of the halides and weaker than that of methide or hydride. An ordering of the trans influence is suggested to be $Cl < Br < I < P \simeq As < ROCR' < Pt < H \simeq CH_3 \simeq Ph$ according to the observed ν_{Pt-CH} and ν_{Pt-Cl} frequencies. These results are consistent with the bond distance data in Table VI and with the accepted trend of the trans influence.

Registry No. III, 97336-44-2; IV, 97336-45-3; V, 97336-46-4; Pt, 7440-06-4.

Supplementary Material Available: Tables of final atomic positional parameters and temperature factors, bond distances, bond angles, anisotropic thermal parameters, hydrogen atom parameters, and observed vs. calculated structure factors for III, V, and IV, respectively (72 pages). Ordering information is given on any current masthead page.

Contribution from the Baker Laboratory of Chemistry,
Cornell University, Ithaca, New York 14853

Effects of the Crystal Field upon the Magnetic Behavior of Samarium in the $SmMo_6S_{8-x}Se_x$ Solid Solution

D. C. JOHNSON,* J. M. TARASCON,† and M. J. SIENKO

Received September 25, 1984

The pseudoternary system $SmMo_6(S_{1-x}Se_x)_8$ has been investigated to determine the valence state and the effects of changing the crystal field upon the magnetic behavior of the samarium cation. Mixed solid solutions have been prepared from ultrapure starting elements and characterized by X-ray diffraction, static Faraday susceptibility, and ac superconductivity studies. The end members and the samples with $x = 6$ and 7 were found to be superconducting with $SmMo_6Se_8$ having the highest critical temperature, 6.5 K. Faraday susceptibility studies over the range 2-300 K show essentially Curie law behavior. The data can be fitted to a Curie-Weiss law [$\chi = C/(T + \Theta) + \chi_0$] with $\Theta = 1$ K, indicating that the samarium cations may order magnetically at lower temperatures than studied here. The data can also be fitted to a Curie law [$\chi = C/T + \chi_0$] with equal success, and the magnetic moment obtained for the samarium cation is 25% lower than the value predicted for a Sm^{3+} cation [μ_B(obsd) = 0.60; μ_B(theor) = 0.845]. This reduction in the moment is a result of crystal field effects, as observed for other samarium systems. The moments obtained were found to vary across the solid solution in response to changes in the symmetry of the crystal field.

Introduction

The Chevrel phases exhibit an unusual collection of physical properties: high superconducting critical temperatures, extremely high critical fields, and the coexistence of superconductivity with magnetic ions and magnetic ordering.[1] This remarkable assortment of properties along with the chemical flexibility of these ternary compounds, MMo_6X_8 (M = rare earth (RE), Pb, Sn, Cu, ...; X = S, Se, Te), has resulted in well over 300 publications since the initial report of their synthesis by Chevrel in 1971.[2]

The main building block of the Chevrel phases is the Mo_6X_8 unit in which a distorted cube is formed by eight chalcogen atoms at the cube corners and six molybdenum atoms sit slightly above the face centers, forming an octahedron within the chalcogen cube. Individual Mo_6X_8 units are rotated approximately 25° about the $\bar{3}$ axis of the cube so as to optimize the bonding distance between a general-position chalcogen atom of one cube and a molybdenum of an adjacent cube. The M atoms are positioned between Mo_6X_8 units either on the $\bar{3}$ axis or in a double belt of 12 tetrahedral sites around the $\bar{3}$ axis. There are two types of chalcogen positions: the two cube corners that are on the $\bar{3}$ axis and the other six positions, which are located around the $\bar{3}$ axis. The former are referred to as special positions and the latter as general positions. The structure is illustrated in Figure 1.

In a previous paper, the authors studied the effect of selenium for sulfur replacement in a number of ternary molybdenum chalcogenide systems. In the case where the ternary element is lanthanum, a trivalent cation, a plot of unit cell volume vs. composition showed a negative deviation from Vegard's law, which indicates that ordering of the chalcogens occurs. In a plot of the hexagonal c_h (and a_h) lattice parameters as a function of composition, two straight lines can be drawn to fit the data: one from $x = 0$ to $x = 0.7$ with a slope of 0.11 Å/x unit and another with slope 1.6 Å from $x = 0.8$ to $x = 1.0$. These two lines cross at the composition $x = 0.75$, which corresponds to $LaMo_6S_2Se_6$, i.e. a completely ordered system in which the two sulfur atoms are in the special positions and the six selenium atoms are in the general positions. A calculation that assumes a hard sphere, idealized structure, and perfect ordering (i.e., all the selenium goes into general position sites until $x = 0.75$) qualitatively reproduces the observed behavior.[3]

When we go to ternary elements other than lanthanum, we observe that at first the a_h parameter again rises more steeply than the c_h parameter and subsequently the c_h parameter increases more rapidly. There is no sharp break at $x = 0.75$, as with lanthanum. We take this to mean that the ordering preference of selenium for general-position sites rather than special-position sites is not perfect.

The depth of the minimum in c_h/a_h vs. x is the most telling indicator for the chalcogen ordering, and in Figure 2 we compare the course of the c_h/a_h parameter for six systems: M = La, Eu, Sm, Yb, Pb, and Ag.[3] For lanthanum, the depth of the minimum is greatest and there is a discontinuity at $x = 0.75$. For Sm, Eu,

* To whom correspondence should be addressed at the Central Research and Development Department, Experimental Station, E. I. du Pont de Nemours and Co., Wilmington, DE 19898.
† Bell Communications Research, Murray Hill, NJ 07974.

(1) For reviews of the Chevrel phases see: Yvon, K. *Curr. Top. Mater. Sci.* **1979**, *3*, 53. Fischer, O. *Appl. Phys.* **1978**, *16*, 1.
(2) Chevrel, R.; Sergent, M.; Prigent, J. *J. Solid State Chem.* **1971**, *3*, 515.
(3) Johnson, D. C.; Tarascon, J. M.; Sienko, M. J. *Inorg. Chem.* **1983**, *22*, 3773.

0020-1669/85/1324-2808$01.50/0